Spectra of Baroclinic Inertia–Gravity Wave Turbulence

ROMAN E. GLAZMAN

Jet Propulsion Laboratory, California Institute of Technology, Pasadena, California

(Manuscript received 13 February 1995, in final form 11 December 1995)

ABSTRACT

Baroclinic inertia–gravity (IG) waves form a persistent background of thermocline depth and sea surface height oscillations. They also contribute to the kinetic energy of horizontal motions in the subsurface layer. Measured by the ratio of water particle velocity to wave phase speed, the wave nonlinearity may be rather high. Given a continuous supply of energy from external sources, nonlinear wave–wave interactions among IG waves would result in inertial cascades of energy, momentum, and wave action. Based on a recently developed theory of wave turbulence in scale-dependent systems, these cascades are investigated and IG wave spectra are derived for an arbitrary degree of wave nonlinearity. Comparisons with satellite-altimetry-based spectra of surface height variations and with energy spectra of horizontal velocity fluctuations show good agreement. The well-known spectral peak at the inertial frequency is thus explained as a result of the inverse cascade. Finally, we discuss a possibility of inferring the internal Rossby radius of deformation and other dynamical properties of the upper thermocline from the spectra of SSH variations based on altimeter measurements.

1. Introduction

Possible mechanisms of inertia–gravity (IG) wave generation include tidal forcing, atmospheric pressure and wind stress fluctuations, and various types of hydrodynamic instability of vortical oceanic motions. Due to these, virtually permanent, sources of energy IG waves form a persistent background of ocean oscillations. However, with respect to large-scale ocean circulation, open-ocean IG waves (as opposed to coastal and equatorial trapped waves) are usually considered to be of little importance. For example, for numerical modeling, these waves, especially the fast barotropic mode, represent "computational noise" that has to be filtered out; for example, by employing a rigid-lid condition at the surface. One factor that might increase importance of open-ocean IG waves is nonlinear wave–wave interactions resulting in spectral fluxes of energy (as well as action and momentum), hence in a broad spectrum of sea surface height (SSH) and ocean current fluctuations. Oceanographic implications of these fluxes are discussed in section 5. Finally, IG wave turbulence offers a plausible explanation of the peculiar shape of SSH spectra known from satellite altimeter observations—as discussed in sections 5 and 6.

In the present work, based on a heuristic analysis of nonlinear resonant interactions between IG waves (section 3), spectral distributions of wave energy and surface height variations are derived. As indicated in section 5, wave turbulence can develop only in baroclinic modes (we use the Boussinesq approximation) and may be rather strong. Predicted spectra are analyzed in sections 4 and 5 and comparisons with in situ and satellite altimeter measurements are provided.

In the range of scales containing a Rossby radius of deformation, IG waves are characterized by a rather complicated dispersion law:

$$\omega^2 = f^2 + C_{0,m}^2 k^2, \tag{1}$$

where $k = |\mathbf{k}|$, f is the Coriolis parameter (considered to be constant), and $C_{0,m}$ is the phase velocity of Kelvin waves for vertical mode number m. A special case of $m = 0$ corresponds to barotropic waves with $C_{0,0} = \sqrt{gH}$, where H is the (constant) ocean depth. Short- and long-wave asymptotics of (1) are obtained, respectively, for wavenumbers much greater and much smaller than the inverse Rossby radius

$$R_m^{-1} = \frac{f}{C_{0,m}}. \tag{2}$$

For simplicity, we shall limit our consideration to the lowest baroclinic mode and ignore its possible interactions with other vertical modes. Thus, we shall omit subscript m in the subsequent equations. This case would be most appropriate for a two-layer fluid.

The presence of characteristic scale R in (1) makes the problem of nonlinear waves highly nontrivial. In the short-wave approximation and for the lowest degree of nonlinearity, the wave spectrum was derived (Falkovich and Medvedev 1992) by taking advantage of

Corresponding author address: Dr. Roman E. Glazman, Jet Propulsion Laboratory, MS 300-323, 4800 Oak Grove Drive, Pasadena, CA 91109-8099.
E-mail: reg@pacific.jpl.nasa.gov

an approximate scale-invariance of the collision integral. As shown in section 3, these assumptions represent an oversimplification with respect to ocean waves. Therefore, we employ an alternative approach called the multiwave interaction theory. Developed originally for deep water gravity and capillary–gravity waves (Glazman 1992, 1993, 1995), it does not require either scale invariance or weak nonlinearity. However, the heuristic nature of this theory makes it difficult to estimate the range of its validity. The experimental data presented in sections 4 and 5 seem to corroborate the theoretical predictions, although some issues remain unresolved. The most difficult one is the dependence of the effective number of the resonantly interacting wave components on appropriate external factors controlling the degree of the wave nonlinearity.

For the reader unfamiliar with the subject, a few relevant concepts on wave turbulence are sketched in the next section. This presentation is rather qualitative and is focused on physical ideas; a more rigorous and detailed account of this material is available in the special literature (e.g., Zakharov 1984; Zakharov et al. 1992).

2. IG wave turbulence: An overview

The motion equations for a shallow layer of a rotating fluid are

$$\left(\frac{\partial}{\partial t} + \mathbf{U}\cdot\nabla\right)\mathbf{U} + f\hat{\mathbf{k}}\times\mathbf{U} = -g\nabla\zeta$$

$$\frac{\partial\zeta}{\partial t} + \nabla\cdot((H+\zeta)\mathbf{U}) = 0. \qquad (3)$$

Here $\mathbf{U}$ is the horizontal velocity vector averaged over the layer depth H, and $\hat{\mathbf{k}}$ is the unit vector along the earth rotation axis. For simplicity, the Coriolis parameter is assumed to be constant (f-plane approximation) and the gravity force $\mathbf{g}$ parallel to $\hat{\mathbf{k}}$. Therefore, our consideration applies to midlatitudes.

For the case of baroclinic waves, which we discuss in terms of a two-layer model, g in (3) is the reduced gravity g' (in which the prime is dropped): $g' = g(\rho_1 - \rho_2)/\rho_1$. Depth H is then related to the depths of the upper and lower layers by $H = H_1H_2/(H_1 + H_2)$, and $H_1 + \zeta(\mathbf{x}, t)$ is the interface between the two layers—the instantaneous thermocline depth. We also assume $H_1 \ll H_2$ and H_1 to be sufficiently large compared to the amplitude of $\zeta(\mathbf{x}, t)$ oscillations. The free surface plays a passive role: its undulations mimic oscillations of the thermocline boundary—although with a much smaller amplitude and opposite sign (e.g., LeBlond and Mysak 1978, Chapters 16 and 17; Gill 1982, §6.2). Therefore, we shall sometimes refer to oscillations of the thermocline boundary as surface height oscillations—implying that their spectra are identical (up to a constant factor).

We are interested in stationary wave solutions of (3) whose general form is given by $\zeta(\mathbf{x}, t) = \int e^{i(\mathbf{k}\cdot\mathbf{x}+\omega(\mathbf{k})t)}dZ(\mathbf{k})$ with $dZ(\mathbf{k})$ representing a spectral increment of the surface height's (or thermocline boundary's) complex amplitude. A similar expression can be written for the velocity field. The presence of advective terms in (3) leads to the energy exchange among Fourier components. As a result, the wave field exhibits a highly complicated (random) behavior. An appropriate description of such fields is provided by their statistical moments. The simplest such characteristic is the power spectrum $F_\zeta(\mathbf{k})$ of $\zeta(\mathbf{x}, t)$ variations

$$F_\zeta(\mathbf{k}_1)\delta(\mathbf{k}_1 - \mathbf{k})d\mathbf{k}_1 d\mathbf{k} = \langle dZ(\mathbf{k})dZ^*(\mathbf{k}_1)\rangle, \qquad (4)$$

where the angle brackets denote ensemble averaging. This implies statistical spatial homogeneity of field $\zeta(\mathbf{x}, t)$. Subscript ζ becomes useful in sections 4 and 5—when we analyze kinetic and potential energy spectra.

A statistically stationary wave field is observed if the external source, supplying energy at a constant rate, works long enough to result in a steady spectral flux of wave energy (and of other integrals conserved in the spectral cascade). In many problems of wave turbulence the external input is considered to be confined to a narrow band of wavenumbers/frequencies. In other words, outside the "generation range" the spectral fluxes are assumed to be purely inertial. Similarities with the 3D or 2D eddy turbulence in an incompressible fluid are obvious. For instance, the energy flux toward high wavenumbers is identified with the rate of energy dissipation (as in 3D turbulence) and an inverse spectral cascade is possible (as in 2D turbulence) (Zakharov 1984). There are also considerable differences between eddy and wave turbulence. In particular, wave turbulence depends on the intrinsic relationship between wavenumber $\mathbf{k}$ and frequency ω. For eddy turbulence, dispersion relationships do not exist. Similar to the case of surface gravity waves on deep water, (1) forbids three-wave resonant interactions. The lowest-order resonance occurs in wave tetrads

$$\mathbf{k}_1 \pm \mathbf{k}_2 \pm \mathbf{k}_3 \pm \mathbf{k}_4 = 0$$

$$\omega_0 \pm \omega_2 \pm \omega_3 \pm \omega_4 = 0. \qquad (5)$$

The formal, small-perturbation theory describes this type of processes in the framework of the kinetic equation (Hasselmann 1962; Zakharov et al. 1992), which is usually written for the spectral density of wave action, $N(\mathbf{k}, t) = F(\mathbf{k}, t)/\omega$, where $F(\mathbf{k}, t)$ is the energy spectrum. The relationship between $F(\mathbf{k}, t)$ and $F_\zeta(\mathbf{k}, t)$ may be rather complicated. For the inertial interval, the kinetic equation in the approximation of four-wave interactions is

$$\partial N(\mathbf{k}, t)/\partial t = \int |T_{0123}|^2\delta(\omega + \omega_1 - \omega_2 - \omega_3) \times \delta(\mathbf{k} + \mathbf{k}_1 - \mathbf{k}_2 - \mathbf{k}_3)f_{k123}d\mathbf{k}_1\mathbf{k}_2\mathbf{k}_3, \qquad (6)$$

in which $f_{k123} = N_k N_1 N_2 N_3 (1/N_k + 1/N_1 - 1/N_2 - 1/N_3)$ and the subscripts designate arguments (such as $\mathbf{k}$, $\mathbf{k}_1$, etc.). The integral describes "collisions" that result in the "birth" of two waves in place of two initial waves. Other types of collisions are neglected. The matrix element T_{k123} is a complicated function of wavenumber vectors and frequencies. Its explicit expression for IG waves is given by Falkovich and Medvedev (1992).

Considering the spectral cascade of wave action, we shall treat the integral in (6) as the divergence (in the wavenumber space) of the wave action flux $\mathbf{P}$. To emphasize this interpretation, we shall use the Phillips [1985 and 1977, Eq. (4.8.9)] symbolic notation

$$\int |T_{0123}|^2 \delta(\omega + \omega_1 - \omega_2 - \omega_3)\delta(\mathbf{k} + \mathbf{k}_1 - \mathbf{k}_2 - \mathbf{k}_3) \times f_{k123} d\mathbf{k}_1 \mathbf{k}_2 \mathbf{k}_3 = \nabla_{\mathbf{k}} \cdot \mathbf{P}(\mathbf{k}, t).$$

Assuming that a steady state can be reached (i.e., $\partial N/\partial t = 0$), (6) becomes

$$\nabla_{\mathbf{k}} \cdot \mathbf{P}(\mathbf{k}, t) = 0. \tag{7}$$

Its 1D version—obtained by integrating (7) as $\int_{-\pi}^{\pi} (\cdots) k d\theta$—gives the conservation of the wave action in the spectral cascade, $\partial P(k)/\partial k = 0$, or

$$P(k) = P_0, \tag{8}$$

where P_0 is a constant input flux at, say, $k = k_0$. This conservation law is approximate and is relevant only for nonlinear dynamics dominated by resonant tetrad interactions (5).

A similar expression is obtained for the energy flux by multiplying (6) by $\omega(k)k$ and integrating over azimuthal angle. For the inertial range of the direct energy cascade the result is $\partial Q(k)/\partial k = 0$, or

$$Q(k) = Q_0, \tag{9}$$

where Q_0 is the rate of energy input. In contrast to (8), this conservation law is exact and it holds for an arbitrary number of the resonantly interacting Fourier components.

Equation (6) may have several stationary solutions (Zakharov 1984). However, some of them may be physically meaningless. In the case of weakly nonlinear, sufficiently short IG waves, (1) can be replaced with

$$\omega \approx C_0 k \left(1 + \frac{1}{2}(kR)^{-2}\right). \tag{10}$$

Falkovich and Medvedev (1992) showed that, in this approximation, (6) has two physically meaningful solutions, corresponding to two types of spectral cascade: the inverse cascade of wave action and the direct cascade of wave energy. In what follows, we assume that both cascades are local in the wavenumber space. Validity of this assumption with respect to the direct energy cascade is discussed in section 3.

So far, equations of type (6) yielded closed-form solutions only for scale-invariant systems characterized by simple dispersion laws and simple expressions for the wave energy. Scale invariance leads to drastic simplifications of the matrix element T_{k123}, which becomes a homogeneous function of $\mathbf{k}$: $T(\lambda\mathbf{k}, \lambda\mathbf{k}_1, \lambda\mathbf{k}_2, \lambda\mathbf{k}_3) = \lambda^m T(\mathbf{k}, \mathbf{k}_1, \mathbf{k}_2, \mathbf{k}_3)$. As a result, power-law solutions $F(k) \propto k^{-s}$ become possible. For short (but not too short) waves, an approximate solution corresponding to the inverse cascade of wave action is

$$F(k) \propto P_0^{1/3} k^{-10/3} \tag{11}$$

(Falkovich and Medvedev 1992). This is a 2D spectrum of wave energy in which the angular dependence is omitted (being assumed constant). Solution (11) is valid only for a very narrow range of wavenumbers in which the reduced dispersion (10) is substantially stronger than the wave nonlinearity (as required by the small-perturbation theory). In section 3, we provide a more general result for the inverse cascade.

When the nonlinearity is greater than that implied in the lowest-order theory, the derivation of a kinetic equation (to account for higher-order terms in the perturbation series) becomes impractical. However, as an introduction to the heuristic arguments of section 3, it is useful to review some qualitative aspects of the formal perturbation theory. Suppose the perturbation expansion is carried to an arbitrary order. The first nonlinear terms in deterministic equations [for properly normalized Fourier amplitudes $a(\mathbf{k}, t) \sim O(\epsilon)$], are of order ϵ^2 and the subsequent terms are of order ϵ^3, ϵ^4, etc., where ϵ is the measure of the nonlinearity. For most wave problems, including IG waves, $\epsilon = u/c$, where u is the characteristic velocity of water particles and c is the wave phase speed (for a given wavelength). Suppose further that, based on the dynamical equations (and assuming random forcing), one can derive a closed-form kinetic equation for statistical moments such as $\langle a(\mathbf{k}, t) a^*(\mathbf{k}_1, t)\rangle$. In terms of the action transfer, this equation could be written symbolically as

$$\frac{\partial N(\mathbf{k}, t)}{\partial t} + I^{(3)} + I^{(4)} + I^{(5)} + \cdots = \gamma(\mathbf{k}) N(\mathbf{k}, t), \tag{12}$$

where "partial collision integrals" $I^{(n)}$ account for n-wave interactions. If three-wave interactions are nonresonant, term $I^{(3)}$ is eliminated by an appropriate canonical transformation of the Hamiltonian. This, however, is relevant only to weakly nonlinear waves (Zakharov et al. 1992)—when all terms starting with $n = 5$ are negligible. Apparently, the collision integrals in (12) scale as $\epsilon^{2(n-1)}$. Furthermore, $\gamma(\mathbf{k})N(\mathbf{k}, t)$ represents the external source (or sink, or both) where $\gamma(\mathbf{k})$ is an increment (decrement) of wave growth (attenuation), which is zero in the inertial range. Weakly

nonlinear waves (i.e., $\epsilon \ll 1$) permit neglect of all partial collision integrals except for the first one. Indeed, if $\epsilon \approx 0.1$, the first collision term in (12) is 10^2 times as large as the subsequent terms. However, this is not the case if the nonlinearity is stronger. For a weak inequality $\epsilon < 1$, we would have to retain a series of terms (up to $n \approx 6$ for the case of $\epsilon \approx 0.5$) in order to maintain the same accuracy as in our example with $\epsilon \approx 0.1$. Of course, the numbers should not be taken too literally, for the real situation is more complicated. However, the suggestion that multiwave interactions with $n = 5$, 6, etc., could become as important as the lower-order interactions is plausible. Finally, when $\epsilon \to 1$, interactions of all orders become of comparable importance. This case of strong wave turbulence, with $n \to \infty$, results in "saturated" spectra. Larraza et al. (1990) showed that the Phillips spectrum $F(k) \sim k^{-4}$ for deep water gravity waves is just one example. A similar consideration is presented in (Glazman 1993) for capillary waves, while a monotonous transition from weak to strong turbulence is studied in (Glazman 1995) for scale-dependent capillary–gravity waves. Theoretical and empirical relationships between the effective number of resonantly interacting wave components and the external parameters of the problem are also suggested in those works.

3. Heuristic theory of IG wave turbulence

Let us introduce the "effective number" ν of resonantly interacting Fourier components on the hypothesis that all interactions up to this order make comparable contributions to the spectral flux. The energy transfer equation is obtained by multiplying (12) by $\omega(k)$ and truncating the series of partial fluxes at an appropriate order ν:

$$\frac{\partial F(\mathbf{k}, t)}{\partial t} + \sum_{n=3}^{\nu} \nabla_{\mathbf{k}} \cdot \mathbf{Q}^{(n)} = \gamma(\mathbf{k}) F(\mathbf{k}, t). \quad (13)$$

The use of the flux divergence form $\nabla_{\mathbf{k}} \cdot \mathbf{Q}^{(n)}$ in place of $\omega(k) I^{(n)}$ is justified here because—as mentioned in connection with (9)—the energy is conserved in the direct cascade for an arbitrary number of resonantly interacting wave components. In a steady state (13) reduces to (9) with

$$Q = \sum_{n}^{\nu} Q^{(n)}. \quad (14)$$

The effective number ν of resonant wave components depends on the degree of the wave nonlinearity; hence, it is a monotonously increasing function of the "internal parameter" ϵ and can be, hopefully, related to external factors such as the energy input Q_0. As discussed earlier (e.g., Glazman 1995), parameter ν is a statistical characteristic of the wave process and is not necessarily an integer number.

Considering the energy cascade, one can introduce the amount of energy, E_j, transferred by the local nonlinear interactions from a given narrow range of scales (the jth step in the cascade) to the next (the $j + 1$ step in the cascade):

$$E_j = \int_{k_j}^{k_{j+1}} F(k) k dk,$$

where

$$k_{j+1}/k_j = r \quad (15)$$

and $r > 1$ is a constant. The characteristic time t_j of the spectral transfer at step j, called the turnover time, should be taken as the largest among all individual turnover times associated with partial fluxes in (13). Indeed, it is the slowest process that controls the end result. By scaling the terms in (13), one ultimately finds

$$t_j^{-1} \sim \omega \epsilon^{2(\nu-2)}, \quad (16)$$

where ω is related to k by (1) and $\epsilon \equiv u/c$ is explained in the preceding section.

Expression (16), with $\nu = 4$ and $\epsilon = ak$, where a is the characteristic wave amplitude, was employed by Kitaigorodskii (1983) and Phillips (1985) to re-derive the Zakharov-Filonenko (1966) spectrum of weak turbulence in deep water gravity waves. For an arbitrary ν and $\epsilon = ak$, Eq. (16) was suggested by Larraza et al. (1990).

In terms of (15) and (16), the spectral flux of wave energy is simply

$$Q = E_j/t_j. \quad (17)$$

Obviously, this cascade model of wave turbulence is rather similar to that of eddy turbulence (e.g., Frisch et al. 1978). Remembering (9), we shall use $E_j/t_j = Q_0$ in place of the kinetic equation. Expressing E_j and t_j in terms of k, ν, and other relevant quantities one can estimate the shape of the spectrum. This, however, presumes that the spectrum falls off sufficiently fast as the wavenumber increases (Glazman 1995). Indeed, differentiating (15), $\partial E_j/\partial k_j = -(F(k_j)k_j - F(k_j r)k_j r^2)$, we find

$$F(k_j) \approx -\frac{1}{k_j} \frac{\partial E_j}{\partial k_j}. \quad (18)$$

This approximation is valid if, and only if, the spectrum falls off not slower than k^{-s} where the exponent s satisfies $r^{2-s} \ll 1$. Assuming for now that this condition holds, we shall check it a posteriori.

The kinetic and potential energies of IG waves (per unit mass of water, per unit surface area) are

$$\mathrm{EK} = \frac{\langle |\mathbb{U}|^2 \rangle}{2}, \quad \mathrm{EP} = \frac{g\langle \zeta^2 \rangle}{2H}. \quad (19)$$

For a narrow frequency band between k_j and k_{j+1}, the energies are referenced to the corresponding character-

istic scales of the wave amplitude a_j, wavenumber k_j, etc. (In what follows, we will often omit the subscript j at k_j and ω_j.) The ratio of these energies increases with an increasing wavelength (e.g., Gill 1982). Approximately,

$$\frac{\mathrm{EK}_j}{\mathrm{EP}_j} \approx 1 + \frac{2}{(kR)^2}. \tag{20}$$

Physically, the absence of energy equipartition is because the orbits of water particles are not strictly vertical (as would be the case for pure gravity waves). Their inclination is the greater, the larger the relative importance of the Coriolis force (e.g., LeBlond and Mysak 1978, Fig. 17.1). Since the total energy is $E = \mathrm{EK} + \mathrm{EP}$, it is useful to express both components in terms of E_j:

$$\mathrm{EK}_j \approx \frac{E_j}{2}\left(1 + \frac{1}{1 + (kR)^2}\right) \tag{21a}$$

$$\mathrm{EP}_j = \frac{E_j}{2}\frac{(kR)^2}{1 + (kR)^2}. \tag{21b}$$

In view of (19) and (21a), the characteristic particle velocity at scale k is given by

$$u^2(k) = E_j\left(1 + \frac{1}{1 + (kR)^2}\right). \tag{22}$$

Based on (1), the characteristic phase speed is

$$c^2(k) \approx C_0^2\left(1 + \frac{1}{(kR)^2}\right). \tag{23}$$

We can now express the interaction time t_j in terms of $E_j, k, \omega(k)$, and C_0 [which is the same as $C_{0,m}$ appearing in (1) and (2)]: using (1), (22), and (23) the end result is

$$t_j^{-1} \sim C_0 R^{-1}(1 + \tilde{k}^2)^{1/2}\left[\frac{E_j}{C_0^2}\left(1 - \frac{1}{(1 + \tilde{k}^2)^2}\right)\right]^{\nu-2}, \tag{24}$$

where

$$\tilde{k} = kR \tag{25}$$

is the nondimensional wavenumber. It is also convenient to nondimensionalize other quantities:

$$\tilde{Q}_0 = (R/C_0^3)Q_0, \quad \tilde{E}_j = E_j/C_0^2, \quad \tilde{F}(\tilde{k}) = \alpha_q F(k)/(C_0 R)^2. \tag{26}$$

The last relationship contains a nondimensional constant of proportionality α_q, which plays the same role as the Kolmogorov constant in classical fluid turbulence—it allows us to use sign "=" in the subsequent formulas. With t_j^{-1} given by (24), Eq. (17) can be solved for E_j. In the nondimensional form, the result is

$$\tilde{E}_j = \tilde{Q}_0^{1/(\nu-1)} z^{-1/2(\nu-1)}(1 - 1/z^2)^{-(\nu-2)/(\nu-1)}, \tag{27}$$

where we introduced

$$z = 1 + \tilde{k}^2. \tag{28}$$

According to (1) and (2), this new variable coincides with the squared nondimensional frequency $[\omega(k)/f]^2$.

In terms of z, Eq. (18) takes the form

$$\tilde{F}(\tilde{k}) = -2\left.\frac{\partial \tilde{E}_j}{\partial z}\right|_{z=1+\tilde{k}^2}. \tag{29}$$

This yields the 2D spectrum of the total wave energy

$$\tilde{F}(\tilde{k}) = \frac{\tilde{Q}_0^{1/(\nu-1)}}{(\nu - 1)} z^{(\nu-7/2)/(\nu-1)} \times (z^2 - 1)^{-(2\nu-3)/(\nu-1)}(z^2 + 4\nu - 9). \tag{30}$$

In order to investigate the validity of the present theory at high wavenumbers, we need the short-wave asymptotic of (30). This is given by

$$\tilde{F}(\tilde{k}) \propto \tilde{k}^{-s}(1 + 4\nu\tilde{k}^{-4}), \tag{31}$$

where $s = 2 + 1/(\nu - 1)$. Obviously, the necessary condition for (18) to be valid is $s > 2$. A strong inequality, $s \gg 2$, means that the spectral cascade is local. This is so because the spectral width of a cascade step [measured by parameter r of (15)] does not have to be very large in order to satisfy the requirement $r^{2-s} \ll 1$. At high $\tilde{k}$—as follows from (31)—the locality of wave–wave interactions comes into question because we only have a weak inequality $s > 2$. Therefore, in the high-wavenumber range our simple theory needs to be complemented with a model of energy dissipation due to an intermittent breaking of steep wavelets. Such a model would describe a nonlocal energy transfer to small scales, similar to that observed in deep water gravity waves.

For weakly nonlinear waves (when $\nu = 4$), an additional physically meaningful stationary solution of (6) corresponds to the inverse cascade of wave action (8). This solution is found based on the conservation of the action flux, that is,

$$N_j/t_j = P_0, \tag{32}$$

where $N_j = \int_{k_n}^{k_{n+1}} F(k)\omega^{-1}kdk$. In the same fashion as before, we arrive ultimately at

$$\tilde{F}(\tilde{k}) \approx \frac{8}{3}\tilde{P}_0^{1/3} z^{1/3}(z^2 - 1)^{-5/3}, \tag{33}$$

where $\tilde{P}_0 = \alpha_p P_0/C_0^2$. The Kolmogorov constant α_p generally differs from α_q introduced in (26), and the ratio of these constants can be set based on the requirement that the spectra corresponding to the direct and inverse cascades match at common wavenumbers. Figure 1 compares the energy spectrum (33) with the spectrum (11) based on the approximate dispersion rela-

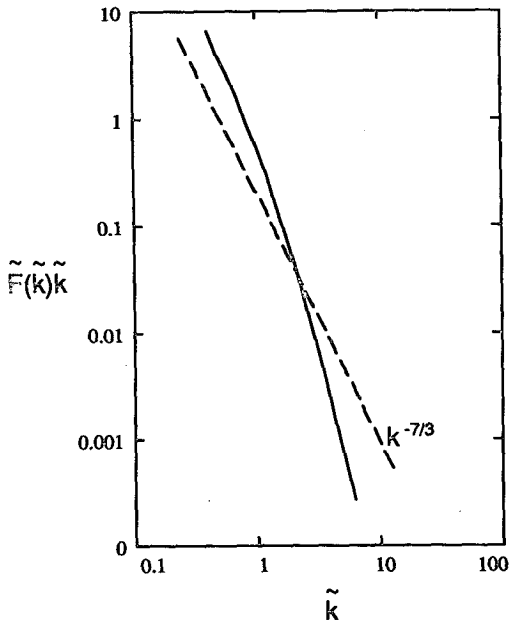

FIG. 1. The nondimensional 1D spectrum of total wave energy based on the inverse cascade of wave action. Solid curve: Eq. (33). Dashed curve: asymptotic solution (11) (Falkovich and Medvedev 1992) plotted as a 1D spectrum $k^{-7/3}$.

tionship (10). We shall plot the results in terms of 1D spectra $\tilde{k}\tilde{F}(\tilde{k})$. This plot gives an idea about the range in which (11) is in an approximate agreement with our prediction; roughly this is $\tilde{k} < 2$. At higher wavenumbers, when the wave dispersion becomes small compared to the wave nonlinearity, the Falkovich–Medvedev theory does not apply.

4. IG wave spectra

The spectra usually reported in experimental literature are based on measurements of surface height and horizontal velocity fluctuations. Therefore, in this section we provide wavenumber and frequency spectra for the kinetic and potential energy densities. The potential energy spectrum $F_p(k)$ is found based on (21b). It differs from the spectrum of surface (i.e., interface) height oscillations only by a dimensional factor: $F_\zeta(k) = (2H/g)F_p(k)$. In the nondimensional form, the surface height spectrum is

$$\tilde{F}_\zeta(\tilde{k}) \sim \frac{\tilde{Q}_0^{1/(\nu-1)}}{2(\nu-1)} \frac{(z-1)(z^2+4\nu-9)}{(z^2-1)^{(2\nu-3)/(\nu-1)} z^{5/2(\nu-1)}}, \quad (34)$$

and its dimensional expression is $F_\zeta = 2(\mathrm{HR})^2\tilde{F}_\zeta$. Our choice of scales makes the nondimensional spectrum of wave potential energy identical to the nondimensional spectrum of surface height variations: $\tilde{F}_p(\tilde{k}) = \tilde{F}_\zeta(\tilde{k})$. Since the angular dependence in our 2D spectra is ignored, the corresponding 1D spectrum of surface height is simply $\tilde{F}_\zeta(\tilde{k})\tilde{k}$. The plot of this spectrum is shown in Fig. 2 for several values of ν.

The spectrum of surface height variations due to the wave action cascade is based on (33). Employing (21b), we find

$$\tilde{F}_\zeta(\tilde{k}) \approx \frac{4}{3}\tilde{P}_0^{1/3} z^{-2/3}(z^2-1)^{-5/3}(z-1). \quad (35)$$

Based on (21a) and (28), kinetic energy spectra F_k are related to the spectra of total wave energy, (30) and (33), by

$$F_k = \frac{1+z}{2z} F. \quad (36)$$

In Fig. 3, these spectra are plotted for both the direct and the inverse cascade: the former is assumed to occur at $\tilde{k} \geq 1.6$ and the latter at $\tilde{k} < 1.6$. To match the two branches at $\tilde{k} \approx 1.6$, we had to multiply (30) and (34) by 1/2, which is equivalent to selecting an appropriate ratio of the Kolmogorov constants. As pointed out in the next section, the example presented in Fig. 3 is relevant to a case of baroclinic inertia–gravity waves generated by a semidiurnal tide in a midlatitude region.

The spectra in Fig. 2 contain interesting information. The first (actually, rather smooth) "break" in the spectrum (at $\tilde{k} \approx 0.8$) tentatively separates the range of inertial oscillations from that strongly affected by the gravity force. The second break (at $\tilde{k} \approx 3$) is pronounced only if the wave nonlinearity is sufficiently high ($\nu \geq 7$). At $0.8 < \tilde{k} < 3$ we have "fully" dis-

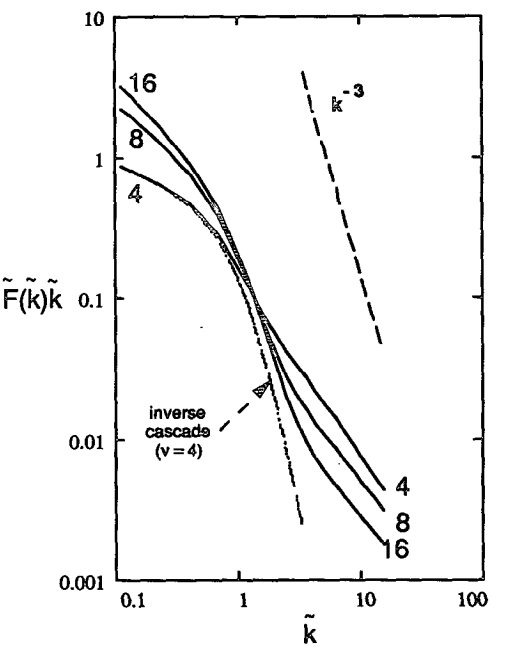

FIG. 2. The nondimensional 1D wavenumber spectrum $\tilde{F}_\zeta(\tilde{k})\tilde{k}$ of the thermocline boundary spatial oscillations. Solid curves: Eq. (34) based on the direct energy cascade. The degree of the wave nonlinearity, in terms of the effective number of the resonantly interacting Fourier components ν, is indicated at each curve. Dotted curve: Eq. (35) based on the inverse cascade of wave action.

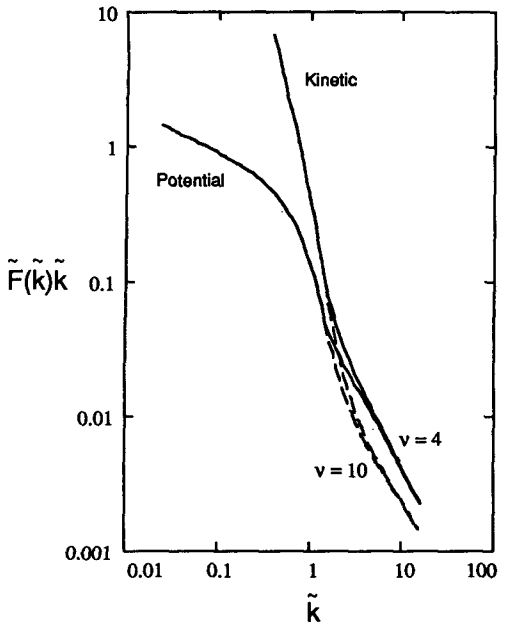

FIG. 3. The nondimensional, composite 1D spectra of kinetic and potential energies. For low wavenumbers ($\tilde{k} \leq 1.6$), the spectra are calculated based on the inverse cascade of wave action: the potential energy spectrum is given by (35), and the kinetic energy spectrum is based on (36) and (33). For high wavenumbers, $\tilde{k} > 1.6$, we used (34) for the potential energy and (35) with (30) for the kinetic energy. Numbers at the curves designate the effective number of resonantly interacting wave components used in the calculations of the direct cascade. Dashed curves represent $\nu = 10$ (highly nonlinear case) for both the kinetic and the potential energy.

persive IG waves whose spectrum is sensitive to the degree of the wave nonlinearity. In this range, the spectrum fall-off may be as fast as k^{-3}, which is faster than in either of the asymptotic regimes of $k \to 0$ or $k \to \infty$. This is the most nontrivial result of the present theory. At $\tilde{k} > 3$, wave dispersion has only a weak effect on the spectrum, and the wave dynamics become dominated by nonlinear factors. This regime of nondispersive ("acoustic") waves is characterized by rather flat spectra [approaching $\sim\tilde{k}^{-1}$ in terms of the 1D spectrum $\tilde{k}\tilde{F}(\tilde{k})\tilde{k}$]. The nonlinearity of such waves is not counteracted by competing factors; hence, it should eventually lead to the formation of "shock" waves accompanied by a vigorous wave breaking. Indeed, spectrum $\tilde{F}(\tilde{k}) \sim \tilde{k}^{-1}$ means that the (1D) surface $\zeta(\mathbf{x})$ is discontinuous in the mean-square sense. Hence, at small scales wave crests tend to become highly asymmetric, having a steep, near-vertical front face and a gentle rear face. In section 6 we discuss implications of this spectral range for dynamical processes in the thermocline.

The frequency spectra can be estimated based on the following relationship between the 2D wavenumber spectrum $F(k)$ and the 1D wave-frequency spectrum $S(\omega)$:

$$S(\omega) = \left[\frac{kdk}{d\omega} F(k)\right]_{k=k(\omega)}. \tag{37}$$

In particular, the nondimensional frequency spectrum corresponding to (30) is found to be

$$\tilde{S}(\tilde{\omega}) = \frac{\tilde{Q}_0^{1/(\nu-1)}\, \tilde{\omega}^{(3\nu-8)/(\nu-1)}(\tilde{\omega}^4 + 4\nu - 9)}{(\nu - 1)\,(\tilde{\omega}^4 - 1)^{(2\nu-3)/(\nu-1)}}. \tag{38}$$

The kinetic and potential energy spectra are

$$\tilde{S}_k(\tilde{\omega}) = \tilde{S}(\tilde{\omega})\frac{\tilde{\omega}^2 + 1}{2\tilde{\omega}^2} \tag{39a}$$

$$\tilde{S}_p(\tilde{\omega}) = \tilde{S}(\tilde{\omega})\frac{\tilde{\omega}^2 - 1}{2\tilde{\omega}^2}. \tag{39b}$$

Like most results of the present approach, these formulas are approximate because we use dispersion law (1) and energy ratio (20) from linear theory and scaling relationships, (18) and (24), in place of a rigorous kinetic equation.

For the direct energy cascade $\tilde{S}_k(\tilde{\omega})$ is plotted in Fig. 4 based on (38) and (39a). However, it is easy to show that at $\tilde{\omega} \leq 1.8$ the kinetic energy spectrum based on the inverse cascade of wave action is almost identical to the spectrum based on (38). Therefore, one can view the spectra in Fig. 4 as consisting of two branches joined at $\tilde{\omega} \approx 1.8$—similar to the composite spectra reproduced in Fig. 3.

A case of weak wave turbulence is presented in Fig. 4 by the solid curve for which $\nu = 4$, while the dashed curve illustrates a higher degree of wave nonlinearity: $\nu = 8$. Evidently, the influence of the wave nonlinearity on the spectrum shape is weaker here than in the case

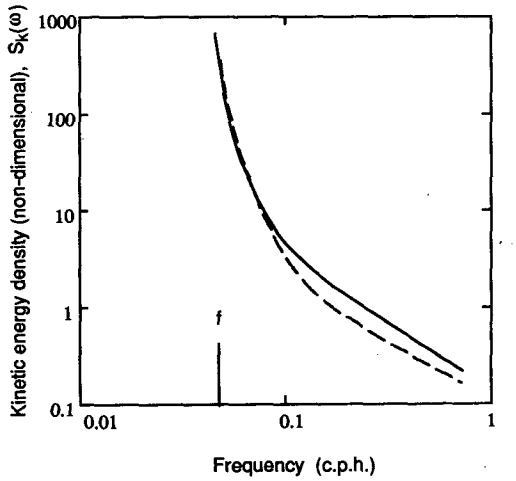

FIG. 4. Theoretical nondimensional frequency spectra of the kinetic energy of horizontal motions caused by baroclinic IG wave turbulence, as based on (38) and (39a). The vertical axis is in arbitrary nondimensional units of the spectral density, and the horizontal axis is the dimensional frequency obtained from $\tilde{\omega}$ as $(\tilde{\omega}/2\pi)2\Omega \sin(\theta)$. Solid curve: $\nu = 4$; dashed curve: $\nu = 8$.

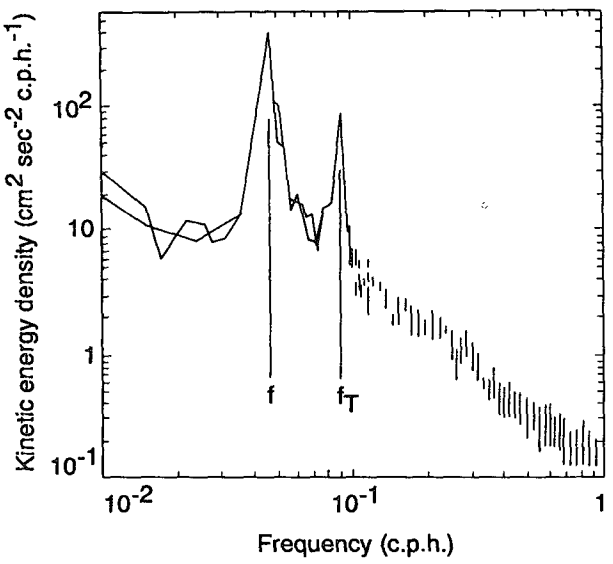

FIG. 5. Frequency spectra of the kinetic energy of horizontal motions measured in the western Sargasso Sea by Gould et al. (1974) using subsurface moorings. The local inertial frequency is marked by f, the semidiurnal tide frequency by f_T. Additional discussion of this plot is provided by Phillips (1977, p. 205).

of wavenumber spectra in Fig. 2. In order to compare (39a) to the experimental spectra presented in Fig. 5, we plotted $\tilde{S}_k$ versus dimensional frequency $(\tilde{\omega}/2\pi)2\Omega \sin(\theta)$ in cph, where Ω is the earth's rotation frequency. The vertical (nondimensional) axis in Fig. 4 is in arbitrary units. Comparing Figs. 4 and 5, one finds that the theoretical spectrum is in good agreement with observations—except, of course, for the narrow frequency band centered around the tidal frequency f_T. Thus, the well-known spectral peak at the inertial frequency is due to the inverse cascade of wave action. Alternative explanations are also available (e.g., Pollard 1970; Munk 1980). Apparently, Fig. 5 lends support to the idea that the tidal energy may provide sufficient input to maintain spectral fluxes in the inertial subranges of IG wave turbulence. This point will be further explored in the next section.

5. Analysis of sea surface height spectra

To some extent, the present work was inspired by satellite altimeter observations showing that power spectra of the SSH field often exhibit features of scale-dependent wave turbulence, such as breaks in power laws and dependence on the intrinsic scale of the problem (the Rossby radius). However, the IG wave turbulence represents only one, not necessarily dominant, component of the total SSH variability. Filtering out fast SSH oscillations (with periods under one day), this component disappears (Glazman et al. 1996). In the wavenumber range of our interest, the spectra of slow motions are strongly influenced by baroclinic Rossby waves and 2D vortical flows (Glazman et al. 1996).

One-dimensional spectra of SSH spatial variations are presently well documented (e.g., Fu 1983; Gaspar and Wunsch 1989; De Mey and Menard 1989; Le Traon et al. 1990, 1994), and 2D spectra and spatial-temporal autocorrelation functions are beginning to be reported (Glazman et al. 1996). These statistical characteristics are based on SSH data from which time-invariant spatial trends have been removed (for instance, by subtracting from each SSH measurement the mean value found by averaging over the period of observations). Typical spectra of these "detrended" SSH variations along satellite passes are presented in Fig. 6, reproduced from Le Traon et al. (1994). The spectra are calculated separately for ascending and descending passes and then averaged together. Therefore, they reflect SSH spatial variations observed practically instantaneously. Really, it takes only about 3 minutes for a satellite to sample a 1000-km groundtrack segment. At wavenumbers above the first spectral break, these spectra appear to be in good agreement with the theoretical

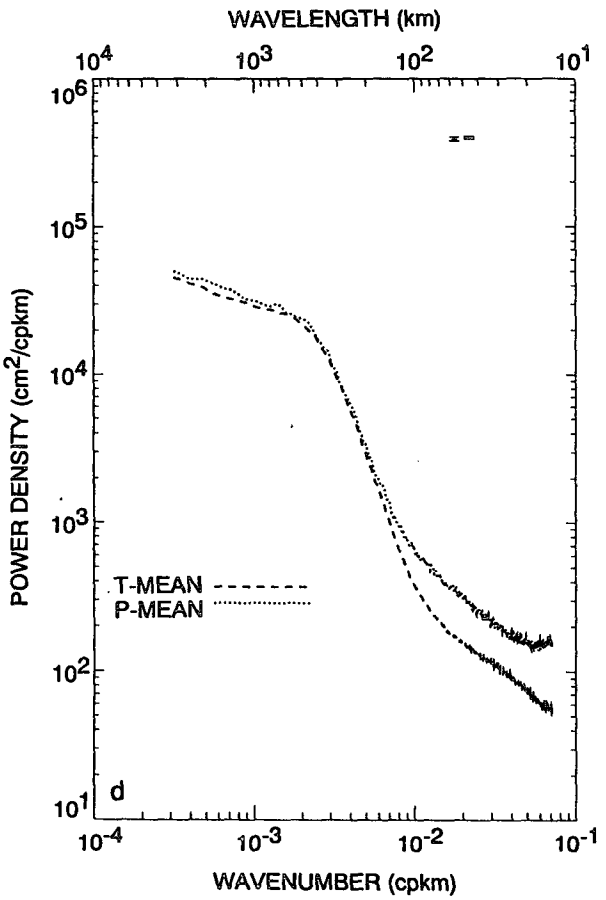

FIG. 6. 1D spectra of SSH spatial variations along altimeter groundtracks (LeTraon et al. 1994) based on Topex/Poseidon data for midlatitude regions (courtesy of the authors).

prediction (34) for the direct energy cascade. Spectrum (35) based on the inverse cascade agrees with observations at wavenumbers roughly below $\tilde{k} = 2$, as shown in Fig. 3.

The observed trends can be explained as follows. Depending on the energy source, the relative extent of the inverse and direct cascade ranges may vary. Suppose that the baroclinic IG wave energy is generated by barotropic tides (scattering at the ocean floor topography). The characteristic wavenumber k_0 for the IG wave energy input is found based on (1), (2) as

$$k_0 = R^{-1}\sqrt{(\omega_{\text{tide}}/f)^2 - 1} = R^{-1}\sqrt{1/\sin^2(\theta) - 1}, \tag{40}$$

where the last equality is valid for a semidiurnal tide. With $\theta = 32^0$ and $R = 40$ km, we find: $k_0 = 0.043$ rad km^{-1}. This example—in which both the direct and the inverse cascades are important—is illustrated in Fig. 3, where we used $\tilde{k}_0 \equiv k_0 R = 1.6$. At $\theta = 50^0$, Eq. (40) would yield $\tilde{k}_0 = 0.8$. Therefore, the relative extent of the direct cascade range would be much greater than in the previous example, and Fig. 2 would be more relevant than Fig. 3. Comparing Figs. 2 and 3, one finds that the overall shape of the spectrum is not much different between these two cases and the positions of the spectrum breaks on the nondimensional wavenumber axis (i.e., $\tilde{k} \approx 0.8$ and $\tilde{k} = 3$) remain unchanged. The actual (dimensional) spectrum is sensitive to the local baroclinic Rossby radius of deformation and the degree of the wave nonlinearity. This is confirmed by spectra estimated for different ocean regions by Le Traon et al. (1990).

Finally, let us emphasize that the theoretical spectra in Figs. 2 and 3 exhibit a relatively slow fall-off as the wavenumber increases: its rate does not exceed k^{-3} and it may be as low as k^{-1}. The SSH spectra based on satellite measurements show a gentle spectral fall-off (k^{-3} and slower) only in the low-energy regions (e.g., Fu 1983; Le Traon et al. 1990). Near the Gulf Stream, for example, the spectra fall off at least as fast as k^{-4}. An explanation of this behavior is simple: in the regions of high mesoscale eddy activity, the SSH variations are dominated by the vortical rather than gravity wave component of fluid motion. The kinetic energy spectra of 2D eddy turbulence are given by k^{-3} or $k^{-5/3}$, corresponding to the enstrophy or energy cascades, respectively (Kraichnan 1967). In terms of 1D spectra of SSH variations $kF_\zeta(k)$, these translate into k^{-5} or $k^{-11/3}$. Such high rates of spectral fall-off are consistently observed in regions of high mesoscale eddy energy (Fu 1983; Le Traon et al. 1990; Glazman et al. 1996).

Apparently, the strong dependence of the (dimensional) wave spectrum on the internal Rossby radius of deformation points to a possibility of inferring this oceanographic parameter from statistical characteristics of SSH variations measured by a satellite altimeter. Moreover, the shape of the spectrum, especially in the high-wavenumber range (Figs. 2, 3, and 6), allows one to estimate the degree of the nonlinearity of baroclinic waves—an important characteristic of dynamical processes in the thermocline.

Comparing potential energy spectra in Figs. 2 and 3 to the spectra in Fig. 6 and to spectra reported for various regions by Le Traon et al. (1990), one concludes that the degree of the wave nonlinearity (in terms of parameter ν) varies from region to region, and may become rather high. This should cause no surprise because the amplitude of the thermocline oscillations (i.e., internal waves) can be rather large: it is known to attain several tens of meters, hence it may constitute an appreciable fraction of the thermocline depth. The physical cause of large-amplitude internal waves is the extremely small difference between the densities of the two layers. This allows large oscillations to be produced by low-energy forcing. The barotropic waves, whose characteristic phase speed is about 200 m s^{-1}, could hardly ever attain a similar degree of nonlinearity.

6. Discussion and conclusions

The present analysis has addressed only the most basic aspects of the problem. By limiting our consideration to a single (first) baroclinic mode we excluded possible exchange of energy with other modes. This exchange may be important, at least within a certain subrange of wavenumbers/frequencies. Further theoretical developments should also include a more elaborate treatment of the Coriolis force (which becomes important for regions closer to the equator) and other factors. Furthermore, since the spectral distribution of energy input to IG wave turbulence is not yet known, our consideration has been limited to purely inertial cascades. In principle, one can generalize the theory to account for a continuous spectral distribution of the external input. Such a generalization would also reduce the uncertainty in the effective value of ν (the number of the resonantly interacting wave components) (Glazman 1992). However, we do not yet have enough knowledge about relevant physical processes to address such issues.

Experimental comparisons indicate that the IG wave spectra in the small-scale range are determined by the direct energy cascade. This has important implications. Specifically, spectral transfer of energy from larger scales should result in energy dissipation at high wavenumbers. This dissipation can occur through a variety of mechanisms of which the internal wave breaking and mixing are most likely. Wave breaking produces small-scale turbulence. For wind-generated surface gravity waves, the probability and other statistics of the wave breaking have been related to the spectrum shape (Snyder and Kennedy 1983; Glazman and Weichman 1989). Therefore, we anticipate that further studies of IG wave turbulence may lead to quantitative charac-

terization of intermittent events of baroclinic wave breaking. Such studies might improve our understanding of vertical fluxes and ocean mixing processes. The plausible suggestion that open ocean tides may provide an energy source for baroclinic IG wave turbulence prompts an interesting question about the role of the inertial cascades in the dissipation of tidal energy and its conversion into other forms of oceanic motions.

The inverse spectral cascade of wave action may play a significant role in large-scale ocean dynamics. The fact that it is responsible for the observed spectral peak of kinetic energy at the inertial frequency—as first suggested by Falkovich (1992)—is confirmed in the present work. Other possible consequences of this cascade are yet to be studied.

The theory indicates that the thermocline oscillations contain important oceanographic information that can be derived from observed SSH spectra. The baroclinic Rossby radius of deformation is just one such item. Another, presently less understood, property is the degree of the wave nonlinearity. This can be inferred by analyzing the spectral slope in different wavenumber subranges.

Acknowledgments. This work was performed at the Jet Propulsion Laboratory, California Institute of Technology, under contract with the National Aeronautics and Space Administration. The authors thanks Dr. Alexander Balk of the Applied Math. Dept. at Caltech for fruitful discussions of this work.

REFERENCES

De Mey, P., and Y. Menard, 1989: Synoptic analysis and dynamical adjustment of GEOS 3 and Seasat altimeter eddy fields in the Northwest Atlantic. *J. Geophys. Res.*, **94**(C5), 6221–6230.

Falkovich, G., 1992: Inverse cascade and wave condensate in mesoscale atmospheric turbulence. *Phys. Rev. Lett.*, **69**, 3173–3176.

——, and S. B. Medvedev, 1992: Kolmogorov-like spectrum for turbulence of inertial–gravity waves. *Europhys. Lett.*, **19**(4), 279–284.

Frisch, U., P.-L. Sulem, and M. Nelkin, 1978: A simple dynamical model of intermittent fully-developed turbulence. *J. Fluid Mech.*, **87**, 719–736.

Fu, L.-L., 1983: On the wavenumber spectrum of oceanic mesoscale variability observed by the Seasat altimeter. *J. Geophys. Res.*, **88**(C7), 4331–4341.

Gaspar, P., and C. Wunsch, 1989: Estimates from altimeter data of baroclinic Rossby waves in the northwestern Atlantic Ocean. *J. Phys. Oceanogr.*, **19**, 1821–1844.

Gill, A. E., 1982: *Atmosphere–Ocean Dynamics.* Academic Press, 662 pp.

Glazman, R. E., 1992: Multiwave interaction theory for wind-generated surface gravity waves. *J. Fluid Mech.*, **243**, 623–635.

——, 1993: A cascade model of wave turbulence with applications to surface gravity and capillary waves. *Fractals*, **1**(3), 513–520.

——, 1995: A simple theory of capillary–gravity wave turbulence. *J. Fluid Mech.*, **293**, 25–34.

——, and P. B. Weichman, 1989: Statistical geometry of a small surface patch in a developed sea. *J. Geophys. Res.*, **94**(C4), 4998–5010.

——, A. Fabrikant, and A. Greysukh, 1996: Statistics of spatio-temporal variations of sea surface height based on Topex altimeter measurements. *Int. J. Remote Sens.*, in press.

Gould, W. J., W. J. Schmitz, and C. Wunsch, 1974: Preliminary field results for a Mid-Ocean Dynamics Experiment (MODE-0). *Deep-Sea Res.*, **21**, 911–932.

Hasselmann, K., 1962: On the non-linear energy transfer in a gravity-wave spectrum. *J. Fluid Mech.*, **12**, 481–500.

Kitaigorodskii, S. A., 1983: On the theory of the equilibrium range in the spectrum of wind-generated gravity waves. *J. Phys. Oceanogr.*, **13**, 816–827.

Kraichnan, R. H., 1967: Inertial ranges in two-dimensional turbulence. *Phys. Fluids*, **10**, 1417–1423.

Larraza, A., S. L. Garrett, and S. Putterman, 1990: Dispersion relations for gravity waves in a deep fluid: Second sound in a stormy sea. *Phys. Rev. A*, **41**(6), 3144–3155.

LeBlond, P. H., and L. A. Mysak, 1978: *Waves In The Ocean.* Elsevier, 602 pp.

Le Traon, P. Y., M. C. Rouquet, and C. Boissier, 1990: Spatial scales of mesoscale variability in the North Atlantic as deduced from Geosat data. *J. Geophys. Res.*, **95**(C11), 20 267–20 285.

——, J. Stum, J. Dorandeu, and P. Gaspar, 1994: Global statistical analysis of Topex and Poseidon data. *J. Geophys. Res.*, **99**(C12), 24 619–24 631.

Munk, W. H., 1980: Internal wave spectra at the buoyant and inertial frequencies. *J. Phys. Oceanogr.*, **10**, 1718–1728.

Phillips, O. M., 1977: *The Dynamics of the Upper Ocean.* 2d ed. Cambridge University Press, 336 pp.

——, 1985: Spectral and statistical properties of the equilibrium range in wind-generated gravity waves. *J. Fluid Mech.*, **156**, 505–531.

Pollard, R. T., 1970: On the generation by winds of inertial waves in the ocean. *Deep-Sea Res.*, **17**, 795–812.

Snyder, R. L., and R. M. Kennedy, 1983: On the formation of whitecaps by a threshold mechanism. Part I: Basic formalism. *J. Phys. Oceanogr.*, **13**, 1482–1492.

Zakharov, V. E., 1984: Kolmogorov spectra in weak turbulence problems. *Handbook of Plasma Physics*, M. N. Rosenbluth and R. Z. Sagdeev, Eds., Elsevier Science, 4–36.

——, and N. N. Filonenko, 1966: The energy spectrum for stochastic oscillation of a fluid's surface. *Dokl. Akad. Nauk SSSR*, **170**, 1292–1295.

——, V. S. L'vov, and G. Falkovich, 1992: *Kolmogorov Spectra of Turbulence I: Wave Turbulence.* Springer-Verlag, 264 pp.